Geometric Tracking of Vehicular mmWave Channels to Enable Machine Learning of Onboard Sensors

Erich Zöchmann*†‡, Vutha Va§, Markus Rupp†, and Robert W. Heath, Jr.§
*Christian Doppler Laboratory for Dependable Wireless Connectivity for the Society in Motion
†Institute of Telecommunications, TU Wien, Austria
‡ Department of Radio Electronics, TU Brno, Czech Republic
§ Wireless Communications and Networking Group, The University of Texas at Austin, USA

***Abstract*—Estimating time-selective millimeter wave wireless channels with directive antennas poses a challenging task. A feasible way of relaxing this channel estimation problem is to focus on the tracking of a few multipath components (MPCs). Aligning antenna beams to the tracked MPCs increases the channel coherence time by several orders of magnitude. We propose to track the MPCs geometrically. Our geometric trackers are based on algorithms known as Doppler-bearing tracking. We reformulate recent work on geometric-polar tracking into an efficient recursive version. If the relative position of the MPCs are known, other sensors on board of a vehicle, for example, lidar, radar, camera, will be capable of performing supervised learning based on their own observed data. Learning the relationship between sensor data and MPCs allows onboard sensors to participate in the channel tracking. Joint tracking from many onboard sensors possibly increases the reliability of the MPC tracking.**

***Index Terms*—Adaptive Filters, Autonomous Vehicles, Directive Antennas, Doppler Measurement, Intelligent Vehicles, Machine Learning, Millimeter Wave Communication**

I. Introduction

Millimeter wave (mmWave) frequency bands are a candidate for vehicular communications already for several decades [1]–[3]. MmWave train-to-infrastructure path loss is measured in [1], mmWave vehicle-to-vehicle communication performance is studied in [2]. Recent advances on mmWave circuit technology [4] renewed the interest in vehicular mmWave communications [3] and for joint vehicular communication and radar [5]. MmWaves offer large bandwidths and render raw-data exchange between vehicles possible [6]. The main concern against vehicular mmWave communications is the direct proportionality of the maximum Doppler shift and the carrier frequency. It was, however, shown theoretically in [7], [8] that directional antennas, anticipated for mmWaves, act as spatial filters. The Doppler effect and hence the time-selectivity is drastically decreased by beamforming. Experimentally, this is demonstrated in [9]. In [10], it was first proposed to utilize the Doppler information for mmWave beam tracking. Measurements in [11] clearly demonstrate that interacting objects, such as overtaking cars, produce distinguishable multipath components in the Doppler profile.

Prior work demonstrates the burden of mmWave channel estimation in a dynamic environment; there seems to be a consensus that channel tracking solves this problem [12]–[21]. By channel tracking, we refer to the process of causal estimation of the current or future direction of the line-of-sight (LOS) component or other strong multipath components (MPCs) based on past measurements. The main benefit of channel tracking is the extended coherence time after successful beamforming. The channel coherence time of the beam-aligned channel is several orders of magnitude longer than for omni-directional reception [7]. A subsequent channel estimation, therefore, runs on a coarser time grid. The work in [13] adopts the idea and the formalism of [12] and directly applies them to THz lens antennas. Extended Kalman filters are used in [14]–[16] to track the beam directions based on channel gain measurements. In [17], it is argued that the road implicitly determines the direction in which a vehicle is to be expected. Beam training is avoided by taking advantage of this prior geometric knowledge. Assuming constant angular acceleration, that is a movement along circles, an algorithm based on the unscented Kalman filter is proposed in [18]. Probabilistic beam tracking is proposed in [19]. In [20], [21] the stochastic Newton's method is applied and these algorithms outperform approaches based on IEEE 802.11ad, and approaches based on compressive sensing [22]; the work in [20], [21] shows a good performance for angular velocities of up to $5^\circ/\mathrm{s}$. In contrast, our proposed algorithm is assessed in scenarios where the angular velocity exceeds $100^\circ/\mathrm{s}$ for a short duration and is on average of about $45^\circ/\mathrm{s}$.

In this contribution, *we propose to track the MPCs geometrically given quantized angular (azimuth) measurements and noisy Doppler observations*. The quantized angular information is obtained by an analog or hybrid beamforming array or a dielectric lense [23]. "Geometric" refers to the (x, y) coordinates originating in the antenna array and the relative velocity $(\dot{x}, \dot{y})$ to the receiver motion. We assume that the transmitter, the receiver, and the interacting objects move without acceleration. Under these assumptions, algorithms performing target-motion analysis by means of Doppler-bearings measurement [24]–[26] are directly applicable. The work in [24]–[27] proposes a formulation called "pseudolinear." By "pseudolinear" we refer to a formulation, where the nonlinearities are either hidden in a measurement (regression) matrix or are lumped with the noise term. This leads to the undesirable consequence of noise correlation of the measurements and the measurement matrix, eventually leading to biased solutions [25]. An early work [24] removes this bias

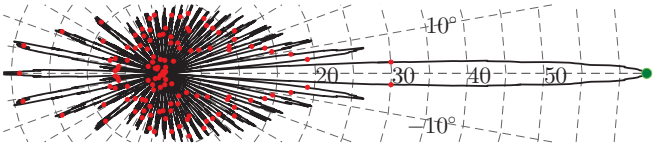

Fig. 1. Beampattern of the proposed uniform circular array with $N = 64$ elements and 4 bit quantization of all steering vectors. The array factor for the desired dirction ($0°$) is marked with a green dot; array factors of all other codebook entries are marked in red.

by the method of instrumental variables. Due to a potential divergence of the instrumental variables approach [26], later work [25], [26] employs the method of total least squares. To apply total least squares, error covariance matrices must be known. Our approach is inspired by [26], but does not need knowledge about the error covariances.

In addition to the excellent angular tracking performance of our algorithm, the obtained geometric information of the MPCs can be utilized to *learn the MPCs from other sensors on board* of automated vehicles [6]. The concept of using external information for improved channel estimation was recently re-introduced, see [28], [29] and the reference therein. Machine learning for configuring wireless links has also been proposed in the context of WLAN and mobile communications [30]–[32]. We emphasize that the actual machine learning implementation is not within the scope of this contribution. This contribution focuses on the formalism to facilitate one possible way of supervised learning for beam tracking.

II. MmWave Equipment and Sensors on Board

We assume a 60 GHz uniform circular array (UCA) with $N = 64$ elements equidistantly spaced on a radius of $r_{\mathrm{UCA}} = {}^{N}\!/_{2} \cdot {}^{\lambda}\!/_{2} \approx 8\,\mathrm{cm}$. The half power beam width is $\theta_{3\mathrm{dB}} \approx {}^{2\pi}\!/_{N} \approx 6°$. The UCA is inherently symmetric in its azimuthal resolution. In contrast to uniform planar arrays, the UCA beam pattern does not change with the pointing direction. To save cost, analog precoding (beamforming) with 4 bit RF phase-shifters is employed. The phase shifts are pre-computed in a codebook spaced by ${}^{\theta_{3\mathrm{dB}}}\!/_{2}$ which gives $\frac{2\pi}{2\pi/N/2} = 2 \cdot 64 = 128$ codebook entries. The beampattern of our UCA pointing towards $0°$ is shown in Fig. 1.

Future, automated cars will perform massive sensing [6]. On board of automated cars, there will be sensors such as global navigation satellite systems (GNSSs), automotive radars (for automatic cruise control and collision detections), lidar (for measuring distances to other objects), and $360°$ camera vision systems. All these sensors have in common that they track objects via target states [33]. At the simplest, this target state consists of the relative (x, y) position and the relative velocities $(\dot{x}, \dot{y})$. If for all of these target states it is known whether they belong to the LOS component or to a specular reflection, the onboard sensors will track the MPCs. The process of associating MPCs to "targets" is illustrated with black circles in Fig. 2. After a successful learning phase, *other sensors on board should later do the channel tracking*. By using machine learning, we can eliminate or significantly

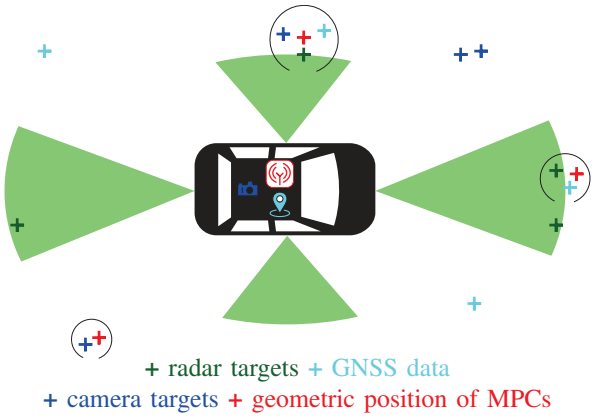

Fig. 2. Supervised learning example. The estimated state vectors of the communication link (red crosses) label the data from other sensors as a valid MPC. Therby online learning of possible beam-direction from other sensors is rendered possible.

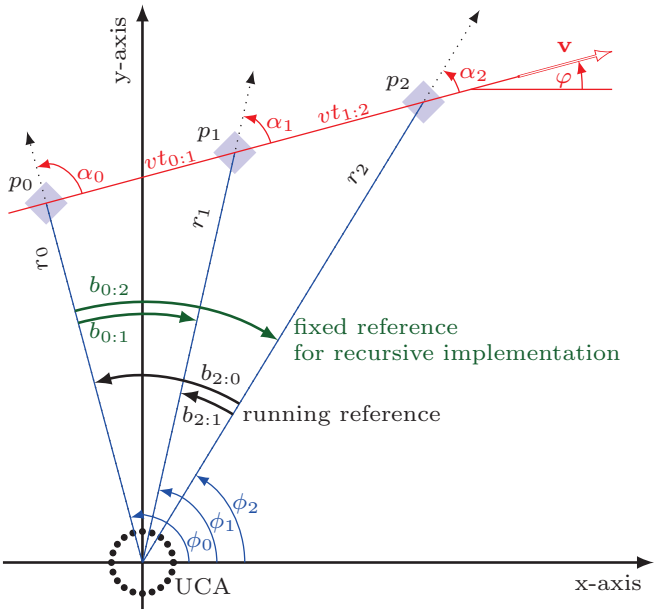

Fig. 3. Geometric relationship of all variables used for the algorithm. The MPC to track is marked as diamond. The UCA is sketched as well.

reduce the beam measurements needed for the currently proposed tracking algorithm.

III. Regression and Projection Model

Our regression model is based on the model proposed in [26]. The main idea of [26] is to track non-accelerating objects on linear trajectories in polar coordinates; target motion analysis in polar coordinates yields a smaller bias than in rectangular coordinates. We hence formulate our model in polar coordinates. This idea is illustrated in Fig. 3. The original tracking problem of [26] uses a running reference (black). Thereby at each time the current state is estimated. This approach produces an increasing system of equations, anew, at any time. In contrast to [26], we use a fixed reference (green) and gather only one new equation per time step. We thereby do not estimate the current state vector; we rather

refine the estimate of the initial state to improve its accuracy over time, as in [24]. Through this reformulation, *the initial state-vector is estimated recursively*. The state vector at current and future times is predicted by a projection.

A. Notation

Matrices $\boldsymbol{Z}$ and vectors $\boldsymbol{z}$ are denoted by bold letters. The all zeros vector (matrix) is expressed by $\mathbf{0}$ and the identity matrix is expressed by $\boldsymbol{I}$. The Euclidean norm is symbolized by $\|\cdot\|$. A quantity defined with a start index i and stop index k is indicated via the subscript $(\cdot)_{i:k}$. Estimated quantities are marked with $\hat{(\cdot)}$. The four-quadrant inverse tangent, is denoted by $\arctan(\cdot,\cdot)$. The dagger $(\cdot)^\dagger$ is used for pseudo inverses and $(\cdot)^{\mathrm{T}}$ is used for transposition.

B. Regression Model

The angle spanning from initial azimuth ϕ_i to the current azimuth ϕ_k is denoted by $b_{i:k}$. In Fig. 3, w.l.o.g. we set $i = 0$. The range (at time k) is denoted by r_k. The time intervals are denoted by $t_{i:k}$. The Doppler relevant angle at time k, that is α_k, is measured from the velocity vector $\boldsymbol{v}$ to the radial speed component. Our main equation is the sine law evaluated for each observation time $k > i$

$$\frac{r_i}{\sin(\alpha_k)} = \frac{v\, t_{i:k}}{\sin(b_{i:k})} \ . \tag{1}$$

Now we reformulate (1) into a so called pseudo-linear formulation [27]

$$\underbrace{[\sin(b_{i:k}),\ -t_{i:k}\cos(b_{i:k}),\ t_{i:k}\sin(b_{i:k})]}_{\boldsymbol{a}^{\mathrm{T}}_{\mathrm{B},i:k}} \underbrace{\begin{bmatrix} r_i \\ v\sin(\alpha_i) \\ v\cos(\alpha_i) \end{bmatrix}}_{\boldsymbol{x}^i} = 0 \ , \tag{2}$$

where all nonlinearities are regressors now. For each observation-time k we obtain one equation in the form of (2). This is written compactly in matrix-vector notation

$$\boldsymbol{A}_{\mathrm{B},i:k}\boldsymbol{x}^i = \mathbf{0} \ . \tag{3}$$

The solution to (3) is not unique. We next exploit Doppler-shift observations ν_k, which are calculated by

$$\nu_k = \frac{v}{\lambda}\cos(\alpha_k) = \frac{v}{\lambda}\cos(\alpha_i - b_{i:k}) \ . \tag{4}$$

Equation (4) is re-written into the same form as (2)

$$\underbrace{\left[0,\ \frac{1}{\lambda}\sin(b_{i:k}),\ \frac{1}{\lambda}\cos(b_{i:k})\right]}_{\boldsymbol{a}^{\mathrm{T}}_{\mathrm{D},i:k}} \underbrace{\begin{bmatrix} r_i \\ v\sin(\alpha_i) \\ v\cos(\alpha_i) \end{bmatrix}}_{\boldsymbol{x}^i} = \nu_k \ . \tag{5}$$

This leads again to a system of equations in form of

$$\boldsymbol{A}_{\mathrm{D},i:k}\boldsymbol{x}^i = \boldsymbol{\nu}_{i:k} \ . \tag{6}$$

We finally arrive at the augmented system of equations

$$\begin{bmatrix} \boldsymbol{A}_{\mathrm{B},i:k} \\ \boldsymbol{A}_{\mathrm{D},i:k} \end{bmatrix} \boldsymbol{x}^i = \begin{bmatrix} \mathbf{0} \\ \boldsymbol{\nu}_{i:k} \end{bmatrix} \ . \tag{7}$$

This system of equations has a unique solution and is called "Doppler-bearing tracking" in the literature [24]–[26]. In this contribution we solve (7) via the method of least squares (LS). Note that (7) is equivalent to

$$\begin{bmatrix} \boldsymbol{A}_{\mathrm{B},i:(k-1)} \\ \boldsymbol{A}_{\mathrm{D},i:(k-1)} \\ \boldsymbol{a}^{\mathrm{T}}_{\mathrm{B},i:k} \\ \boldsymbol{a}^{\mathrm{T}}_{\mathrm{D},i:k} \end{bmatrix} \boldsymbol{x}^i = \begin{bmatrix} \mathbf{0} \\ \boldsymbol{\nu}_{i:(k-1)} \\ 0 \\ \nu_k \end{bmatrix} \ . \tag{8}$$

In (8) we separated the previous observations from the current one. This structure allows for a recursive least squares (RLS) implementation. The recursive estimate of $\boldsymbol{x}^i$ at time k will be denoted by $\hat{\boldsymbol{x}}^i_{i:k}$, in the sequel.

The angular separations $b_{i:k}$ in (1)–(8) are not known and must be estimated. The variable $b_{i:k}$ has to be replaced by $\hat{b}_{i:k}$, the estimated quantity, in the equations above. Such measurement equations are called "errors-in-variables model" in the statistics literature [34]. The estimation of $b_{i:k}$ is initially done by training sequences. For each time k, we estimate the current azimuth angle $\hat{\phi}_k$ by aid of beam sweeping, that is, a codebook scan. All possible beams are iterated and the codebook entry (azimuth direction) with largest receive power is selected. Next we calculate $\hat{b}_{i:k} = \hat{\phi}_k - \hat{\phi}_i$. Later on, onboard sensors might provide the estimate of $\hat{\phi}_k$ and codebook scans can be avoided or at least performed less frequently.

With the estimate of the initial state-vector $\hat{\boldsymbol{x}}^i_{i:k}$, we calculate the initial (x, y) position and the velocity vector $(\dot{x}, \dot{y})$ based on the polar representation.

- $\hat{r}_i$: The range is the first element of the initial state-vector estimate, that is $\hat{\boldsymbol{x}}^i_{i:k}(1)$.
- $\hat{\phi}_i$: The azimuth angle is estimated through designated pilots.
- $\hat{v}$: The velocity calculates through the initial state-vector estimate via $\hat{v} = \sqrt{\left(\hat{\boldsymbol{x}}^i_{i:k}(2)\right)^2 + \left(\hat{\boldsymbol{x}}^i_{i:k}(3)\right)^2}$.
- $\hat{\varphi}$: The angle of the velocity vector to the x-axis is denoted by φ. This angle calculates to $\hat{\varphi} = \hat{\alpha}_i + \hat{\phi}_i = \arctan\left\{\hat{\boldsymbol{x}}^i_{i:k}(2), \hat{\boldsymbol{x}}^i_{i:k}(3)\right\} + \hat{\phi}_i$. (9)

C. Projection Model

A suitable projection from the initial state vector to arbitrary time points was recently derived in [35]. Our assumption of a linear trajectory with non-accelerating MPCs leads to a static velocity vector. Only the range $\hat{r}_i$ and the azimuth angle $\hat{\phi}_i$ need to be projected to current (or future) time points k. The range projection $\hat{r}_k$ is calculated through [35]

$$\hat{r}_k = \left[\hat{r}_i^2 + \left(\hat{v}\, t_{i:k}\right)^2 + 2\hat{r}_i\hat{v}\, t_{i:k}\cos\hat{\alpha}_i\right]^{1/2} = \Bigg[\left(\hat{\boldsymbol{x}}^i_{i:k}(1)\right)^2 + t^2_{i:k}\left(\left(\hat{\boldsymbol{x}}^i_{i:k}(2)\right)^2 + \left(\hat{\boldsymbol{x}}^i_{i:k}(3)\right)^2\right) + 2t_{i:k}\hat{\boldsymbol{x}}^i_{i:k}(1)\hat{\boldsymbol{x}}^i_{i:k}(3)\Bigg]^{1/2}, \tag{10}$$

and the azimuth projection $\hat{\phi}_k$ is calculated through [35]

$$\begin{aligned}\hat{\phi}_k &= \hat{\phi}_i + \arctan\left(\hat{v}t_{i:k}\sin\hat{\alpha}_i, \hat{r}_i + \hat{v}t_{i:k}\cos\hat{\alpha}_i\right) \\ &= \hat{\phi}_i + \arctan\left(t_{i:k}\hat{\boldsymbol{x}}^i_{i:k}(2), \hat{\boldsymbol{x}}^i_{i:k}(1) + t_{i:k}\hat{\boldsymbol{x}}^i_{i:k}(3)\right) \ .\end{aligned} \tag{11}$$

$$\boldsymbol{P}_{i:k} = \begin{cases} \boldsymbol{P}_{i:(k-1)} - \boldsymbol{P}_{i:(k-1)}\boldsymbol{A}_k^{\mathrm{T}}\big(\boldsymbol{I}_{2\times 2} + \boldsymbol{A}_k\boldsymbol{P}_{i:(k-1)}\boldsymbol{A}_k^{\mathrm{T}}\big)^{-1}\boldsymbol{A}_k\boldsymbol{P}_{i:(k-1)}, & \text{for RLS} \\ \boldsymbol{P}_{i:(k-1)} - \boldsymbol{P}_{i:(k-1)}\begin{bmatrix} \boldsymbol{A}_k^{\mathrm{T}} & \boldsymbol{A}_k^{\mathrm{T}} \end{bmatrix}\boldsymbol{R}_{\mathrm{e},i:k}^{-1}\begin{bmatrix} \boldsymbol{A}_k \\ \boldsymbol{A}_k \end{bmatrix}\boldsymbol{P}_{i:(k-1)}, & \text{for } \mathcal{H}_\infty \text{ with} \end{cases} \tag{17}$$

$$\boldsymbol{R}_{\mathrm{e},i:k} = \begin{bmatrix} \boldsymbol{I} & \boldsymbol{0} \\ \boldsymbol{0} & -\gamma\boldsymbol{I} \end{bmatrix} + \begin{bmatrix} \boldsymbol{A}_k \\ \boldsymbol{A}_k \end{bmatrix}\boldsymbol{P}_{i:(k-1)}\begin{bmatrix} \boldsymbol{A}_k^{\mathrm{T}} & \boldsymbol{A}_k^{\mathrm{T}} \end{bmatrix} \tag{18}$$

$$\boldsymbol{P}_{i:k}^{-1} = \begin{cases} \boldsymbol{P}_{i:(k-1)}^{-1} + \boldsymbol{A}_k^{\mathrm{T}}\boldsymbol{A}_k, & \text{for RLS} \\ \boldsymbol{P}_{i:(k-1)}^{-1} + (1-\gamma^{-2})\boldsymbol{A}_k^{\mathrm{T}}\boldsymbol{A}_k, & \text{for } \mathcal{H}_\infty \end{cases} \tag{19}$$

IV. Proposed Robust Recursive Tracker

Our regression model falls in the following time-variant state-space model

$$\boldsymbol{x}_{i:k}^i = \boldsymbol{x}_{i:(k-1)}^i + \boldsymbol{u}_k \tag{12}$$

$$\underbrace{\begin{bmatrix} 0 \\ \nu_k \end{bmatrix}}_{\boldsymbol{y}_k} = \underbrace{\begin{bmatrix} \boldsymbol{a}_{\mathrm{B},i:k}^{\mathrm{T}} \\ \boldsymbol{a}_{\mathrm{D},i:k}^{\mathrm{T}} \end{bmatrix}}_{\boldsymbol{A}_k}\boldsymbol{x}_{i:k}^i + \boldsymbol{n}_k\ , \tag{13}$$

where $\boldsymbol{u}_k$ is a process noise or driving disturbance with unknown distribution. The first component of noise vector $\boldsymbol{n}_k$ stems from the quantization noise of our codebook. The second component is the measurement noise of the Doppler observation and is assumed to be i.i.d. zero mean Gaussian, that is, $\boldsymbol{n}_k(2) \sim \mathcal{N}(0, 100^2)$. The high standard deviation in the Doppler noise term (100 Hz) already takes into account that current mmWave equipment suffers greatly from phase noise, see for example the measurement results in [9], [11]. We assume zero mean Doppler noise as automated cars can use GNSS-disciplined oscillators, so that the carrier frequency offset between cars becomes very small. To increase robustness against quantization effects of our codebook and against the geometry dependent structure of $\boldsymbol{A}_k$, we apply an $\mathcal{H}_\infty$ filter with a finite time horizon [36], [37]. The objective of an $\mathcal{H}_\infty$ filter is to keep the error relation below bounded

$$\sup_{\hat{\boldsymbol{x}}_0^i, \boldsymbol{u}, \boldsymbol{n}} \frac{\sum_{k=i}^N \|\hat{\boldsymbol{x}}_{i:k}^i - \boldsymbol{x}_{i:k}^i\|^2}{\|\hat{\boldsymbol{x}}_0^i - \boldsymbol{x}_0^i\|^2 + \sum_{k=i}^N \|\boldsymbol{u}_k\|^2 + \sum_{k=i}^N \|\boldsymbol{n}_k\|^2} < \gamma^2. \tag{14}$$

The vector $\hat{\boldsymbol{x}}_0^i$ denotes the initial guess of the state vector (in our simulations $\hat{\boldsymbol{x}}_0^i \equiv 0$, $\boldsymbol{u}_k \equiv 0$, and $\gamma = 2$). The $\mathcal{H}_\infty$ filter has a higher error floor and a higher complexity than the plain RLS solution. As we work with a quantized codebook, subsequent measurements potentially provide equal azimuth angle measurements. Due to the structure of $\boldsymbol{a}_{\mathrm{B},i:k}$ and $\boldsymbol{a}_{\mathrm{D},i:k}$ our regression matrix is likely to be rank-deficient, initially. We therefore start with the $\mathcal{H}_\infty$ filter and switch to the RLS filter after we measured three different azimuth angles. The recursive solution to (8) is given as

$$\boxed{\hat{\boldsymbol{x}}_{i:k}^i = \hat{\boldsymbol{x}}_{i:(k-1)}^i + \boldsymbol{P}_{i:k}\boldsymbol{A}_k^{\mathrm{T}}\boldsymbol{H}_{i:k}\big(\boldsymbol{y}_k - \boldsymbol{A}_k\hat{\boldsymbol{x}}_{i:(k-1)}^i\big)}, \tag{15}$$

where

$$\boldsymbol{H}_{i:k} = \begin{cases} \boldsymbol{I}, & \text{for RLS} \\ \big(\boldsymbol{I} + \boldsymbol{A}_k\boldsymbol{P}_{i:k}\boldsymbol{A}_k^{\mathrm{T}}\big)^{-1}, & \text{for } \mathcal{H}_\infty \end{cases}. \tag{16}$$

The covariance matrix $\boldsymbol{P}_{i:k}$ fulfils the recursion (17). By aid of the Woodbury matrix identity, the inverse of the covariance matrix reveals a remarkably simple structure, see (19). Iff $\boldsymbol{P}_{i:k}^{-1}(\gamma)$ is a positive-definite matrix, the possible worst case energy (14) is bounded by γ^2 [37]. Updating $\boldsymbol{P}_{i:k}^{-1}$ and performing an inverse of a symmetric, positive-definite matrix of size 3×3 is more efficient than updating $\boldsymbol{P}_{i:k}$ directly.

V. Performance Bounds - Genie Estimators

Due to quantized angular observations, the already derived Cramér-Rao bound [24] is not applicable. We will compare the obtained estimation results to two other bounds. Firstly, to the "error-free regressors model." Here, we assume that the azimuth angles ϕ_k are perfectly known, hence unquantized, and (3) is utilized without estimates. Secondly, if ϕ_k are known then (3) is not satisfied only in the least-squares sense but determines a solution subspace. In other words, any solution vector $\hat{\boldsymbol{x}}_{i:k}^i$ needs to fulfil

$$\hat{\boldsymbol{x}}_{i:k}^i = \big(\boldsymbol{I} - \boldsymbol{A}_{\mathrm{B},i:k}^{\dagger}\boldsymbol{A}_{\mathrm{B},i:k}\big)\boldsymbol{m}, \qquad \boldsymbol{m} \in \mathbb{R}^3\ . \tag{20}$$

Now, we solve (7) by a nullspace projected solution

$$\hat{\boldsymbol{x}}_{i:k}^{i,\mathrm{NS}} = \arg\min_{\boldsymbol{m}} \big\|\boldsymbol{\nu}_{i:k} - \boldsymbol{A}_{\mathrm{D},i:k}\big(\boldsymbol{I} - \boldsymbol{A}_{\mathrm{B},i:k}^{\dagger}\boldsymbol{A}_{\mathrm{B},i:k}\big)\boldsymbol{m}\big\|\ . \tag{21}$$

As we assume zero mean Gaussian distributed noise for the Doppler measurements $\boldsymbol{\nu}$, the LS solution (21) is the maximum likelihood estimator.

VI. Simulations

For the simulations, we focus on line-of-sight scenarios. Note that our approach works for specular reflections as well. Clustered reflections will lead to a higher uncertainty in determining the azimuth angle. Similar to the IEEE 802.11ad standard, we assume that the TX is transmitting its reference signal omni-directionally. Initially, the RX is scanning all entries from the codebook and determines the direction towards the TX. This procedure is repeated every 20 ms. After the 10^{th} iteration, we use the projection (11) to predict the future azimuth angle. Having the projected azimuth angles at hand, we only check the closest three codebook entries. This gives a performance increase of a factor $(128)/3 \approx 43$ as compared to a full codebook scan.

Our first scenario, entitled "half-overtaking," starts when the overtaking, blue, TX car is at the same height as the slower, red, RX car. The overtaking car has 20 m/s excess speed and

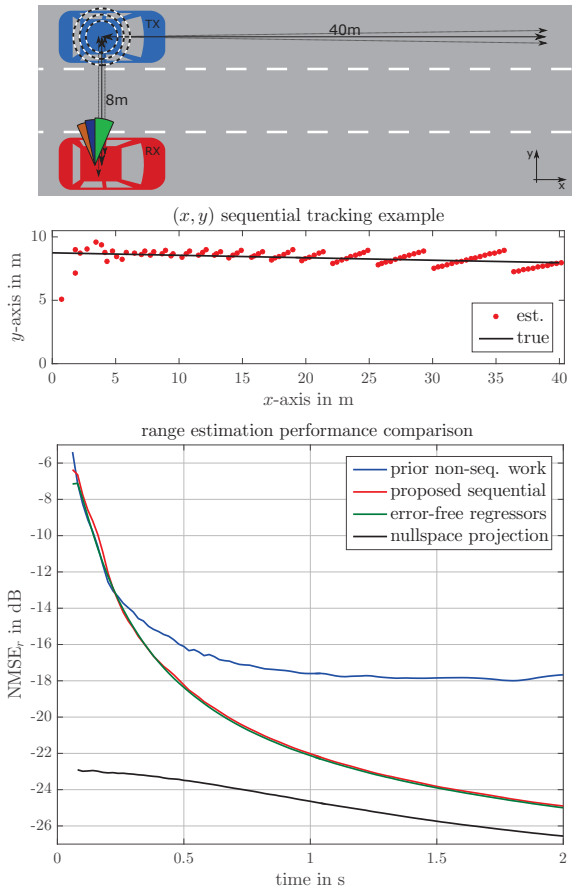

Fig. 4. Half-overtaking manoeuvre: (top) sketch of the scenario (middle) (x, y) positional estimate of the proposed estimator (bottom) normalized mean squared error of the range.

we are observing the TX car for 2 s. In the second scenario, entitled "full-overtaking," the TX starts behind the RX and overtakes with an excess speed of $10\,\mathrm{m/s}$. We observe the manoeuvre for 4 s. The lateral distance was chosen so that the resulting maximum angular velocity ($\omega_{\max} = {}^{v}/_{r_{\min}} = \frac{20\,\mathrm{m/s}}{8\,\mathrm{m}} = \frac{10\,\mathrm{m/s}}{4\,\mathrm{m}} = 2.5\,{}^{\mathrm{rad}}/_{s} \approx 140\,{}^{\circ}/_{s}$) and the resulting mean angular velocity ($\bar{\omega} \approx \frac{\pi/2}{2\,\mathrm{s}} = \frac{\pi}{4\,\mathrm{s}} \approx 0.8\,{}^{\mathrm{rad}}/_{s} = 45\,{}^{\circ}/_{s}$) is equal in both scenarios. We run Monte Carlo simulations with 100 000 runs. To obtain different channel realizations, we vary the lateral distance uniformly in $\Delta r_{\min} \sim \mathcal{U}(-1\,\mathrm{m}, 1\,\mathrm{m})$ around the mean lateral distances, and we vary the angle between both cars uniformly in $\varphi \sim \mathcal{U}(-2^{\circ}, 2^{\circ})$. These variations are drawn in black arrows in Figs. 4 and 5. The normalized mean squared error of the prior work [26], our proposed sequential implementation from Section IV, and both error bounds from Section V for the "half-overtaking" scenario are plotted in the bottom panel of Fig. 4. The top and the middle panel of Fig. 4 show a sketch of the manoeuvre and a scatter plot of the estimated (x, y) position of the proposed sequential estimator for the first Monte Carlo run. Figure 5 shows the corresponding plots of the "full-overtaking" manoeuvre.

Half overtaking turns out to be a not so burdensome than full-overtaking. That's because right from the beginning, the

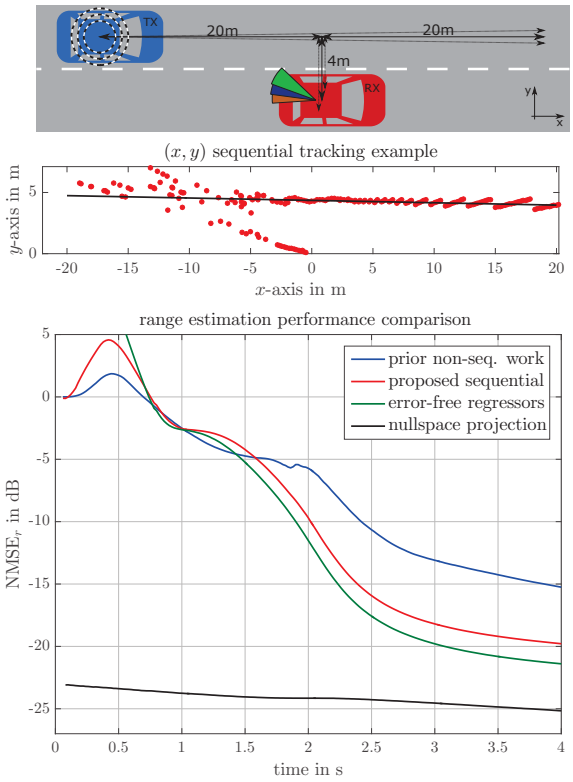

Fig. 5. Full-overtaking manoeuvre: (top) sketch of the scenario (middle) (x, y) positional estimate of the proposed estimator (bottom) normalized mean squared error of the range.

TX car is seen at different azimuth angles and the algorithm convergences fast. The regression model of [26] suffers from a strong bias due the error correlation of the current observation and the regression matrix. Our sequential algorithm outperforms the prior non-sequential modeling approach. The "errors-in-variables" approach comes very close to the error-free regression matrix. Furthermore, there is only a small loss to the nullspace projection. Keep in mind that the "error-free regressors" and the nullspace projection approach make use of exact, unquantized azimuth angles! The full overtaking manoeuvre is characterized by a difficult geometry. At the beginning the TX car is always seen at the same codebook index and the algorithm struggles to converge. In this region the $\mathcal{H}_\infty$ algorithm is used to prevent divergence. After approximately 0.5 s, three different azimuth angles have been measured and the algorithm hands over to RLS. Even with an estimate of the initial state and the covariance matrix, the RLS algorithm needs a considerable time to converge afterwards. The situation is aggravated by the fact that the toughest part (TX car closest to RX car $\rightarrow \omega_{\max}$) comes before convergence sets in. Nevertheless, an acceptable tracking result can be achieved here as well, see the scatterplot in Fig. 5.

VII. Conclusion

Geometric tracking of specular multipath components in vehicular mmWave channels is feasible with low complexity algorithms. Our proposed algorithm achieves good (angular)

tracking even under very dynamic scenarios. It thereby relaxes the time necessary for beam training quite significantly. Furthermore our algorithm outputs a state vector that reflects the relative position and velocity of the multipath components. With this knowledge at hand, it is possible to label the targets visible for other onboard sensors as MPC. Thereby we render one way of supervised learning for these sensors possible.

ACKNOWLEDGMENT

The financial support by the Austrian Federal Ministry of Science, Research and Economy and the National Foundation for Research, Technology and Development is gratefully acknowledged. The research has been co-financed by the Czech Science Foundation, Project No. 17-18675S "Future transceiver techniques for the society in motion," and by the Czech Ministry of Education in the frame of the National Sustainability Program under grant LO1401. This material is based upon work supported in part by the National Science Foundation under Grant No. CNS-1731658 and ECCS-1711702.

REFERENCES

[1] H. Meinel and A. Plattner, "Millimetre-wave propagation along railway lines," *IEE Proceedings F (Communications, Radar and Signal Processing)*, vol. 130, no. 7, pp. 688–694, 1983.

[2] K. Akihito, S. Katsuyoshi, M. Fujise, and S. Kawakami, "Propagation characteristics of 60-GHz millimeter waves for ITS inter-vehicle communications," *IEICE Transactions on Communications*, vol. 84, no. 9, pp. 2530–2539, 2001.

[3] V. Va, T. Shimizu, G. Bansal, and R. W. Heath Jr, "Millimeter wave vehicular communications: A survey," *Foundations and Trends® in Networking*, vol. 10, no. 1, pp. 1–113, 2016.

[4] T. S. Rappaport, J. N. Murdock, and F. Gutierrez, "State of the art in 60-GHz integrated circuits and systems for wireless communications," *Proceedings of the IEEE*, vol. 99, no. 8, pp. 1390–1436, 2011.

[5] P. Kumari, J. Choi, N. G. Prelcic, and R. W. Heath Jr., "IEEE 802.11 ad-based radar: An approach to joint vehicular communication-radar system," *IEEE Transactions on Vehicular Technology*, vol. 67, no. 4, pp. 3012–3027, 2018.

[6] J. Choi, V. Va, N. Gonzalez-Prelcic, R. Daniels, C. R. Bhat, and R. W. Heath Jr., "Millimeter-wave vehicular communication to support massive automotive sensing," *IEEE Communications Magazine*, vol. 54, no. 12, pp. 160–167, 2016.

[7] V. Va, J. Choi, and R. W. Heath Jr., "The impact of beamwidth on temporal channel variation in vehicular channels and its implications," *IEEE Transactions on Vehicular Technology*, vol. 66, no. 6, pp. 5014–5029, 2017.

[8] J. Lorca, M. Hunukumbure, and Y. Wang, "On overcoming the impact of Doppler spectrum in millimeter-wave V2I communications," in *Proc. of IEEE Globecom Workshops (GC Wkshps)*, 2017, pp. 1–6.

[9] E. Zöchmann *et al.*, "Statistical evaluation of delay and Doppler spread in 60 GHz vehicle-to-vehicle channels during overtaking," in *Proc. of IEEE-APS Topical Conference on Antennas and Propagation in Wireless Communications (APWC)*, 2018, pp. 1–4.

[10] E. Zöchmann, S. Caban, M. Lerch, and M. Rupp, "Resolving the angular profile of 60 GHz wireless channels by delay-Doppler measurements," in *Proc. of IEEE Sensor Array and Multichannel Signal Processing Workshop (SAM)*, 2016, pp. 1–5.

[11] E. Zöchmann *et al.*, "Measured delay and Doppler profiles of overtaking vehicles at 60 GHz," in *Proc. of European Conference on Antennas and Propagation (EuCAP)*. EurAAP, 2018, pp. 1–5.

[12] Y. Zhou, P. C. Yip, and H. Leung, "Tracking the direction-of-arrival of multiple moving targets by passive arrays: Algorithm," *IEEE Transactions on Signal Processing*, vol. 47, no. 10, pp. 2655–2666, 1999.

[13] X. Gao, L. Dai, Y. Zhang, T. Xie, X. Dai, and Z. Wang, "Fast channel tracking for Terahertz beamspace massive MIMO systems," *IEEE Transactions on Vehicular Technology*, vol. 66, no. 7, pp. 5689–5696, 2017.

[14] C. Zhang, D. Guo, and P. Fan, "Tracking angles of departure and arrival in a mobile millimeter wave channel," in *Proc. of IEEE International Conference on Communications (ICC)*, 2016, pp. 1–6.

[15] V. Va, H. Vikalo, and R. W. Heath Jr., "Beam tracking for mobile millimeter wave communication systems," in *Proc. of IEEE Global Conference on Signal and Information Processing (GlobalSIP)*, 2016, pp. 743–747.

[16] S. Jayaprakasam, X. X. Ma, J. W. Choi, and S. Kim, "Robust beam-tracking for mmWave mobile communications," *IEEE Communications Letters*, vol. 21, no. 12, pp. 2654–2657, 2017.

[17] A. Loch, A. Asadi, G. H. Sim, J. Widmer, and M. Hollick, "Mm-wave on wheels: Practical 60 GHz vehicular communication without beam training," in *Proc. of 9th International Conference on Communication Systems and Networks (COMSNETS)*, 2017, pp. 1–8.

[18] J. Zhao, F. Gao, W. Jia, S. Zhang, S. Jin, and H. Lin, "Angle domain hybrid precoding and channel tracking for millimeter wave massive MIMO systems," *IEEE Transactions on Wireless Communications*, vol. 16, no. 10, pp. 6868–6880, 2017.

[19] J. Palacios, D. D. Donno, and J. Widmer, "Tracking mm-Wave channel dynamics: Fast beam training strategies under mobility," in *Proc. of IEEE Conference on Computer Communications (INFOCOM)*, 2017, pp. 1–9.

[20] J. Li, Y. Sun, L. Xiao, S. Zhou, and C. E. Koksal, "Super fast beam tracking in phased antenna arrays," *arXiv preprint arXiv:1710.07873*, 2017.

[21] J. Li, Y. Sun, L. Xiao, S. Zhou, and A. Sabharwal, "How to mobilize mmWave: A joint beam and channel tracking approach," *arXiv preprint arXiv:1802.02125*, 2018.

[22] J. Rodríguez-Fernández, N. Gonzáiez-Prelcic, and R. W. Heath Jr., "Frequency-domain wideband channel estimation and tracking for hybrid MIMO systems," in *Proc. of 51st Asilomar Conference on Signals, Systems, and Computers*, 2017, pp. 1829–1833.

[23] Y. Zeng and R. Zhang, "Millimeter wave MIMO with lens antenna array: A new path division multiplexing paradigm," *IEEE Transactions on Communications*, vol. 64, no. 4, pp. 1557–1571, 2016.

[24] Y. Chan and S. Rudnicki, "Bearings-only and Doppler-bearing tracking using instrumental variables," *IEEE Transactions on Aerospace and Electronic Systems*, vol. 28, no. 4, pp. 1076–1083, 1992.

[25] K. Ho and Y.-T. Chan, "An asymptotically unbiased estimator for bearings-only and Doppler-bearing target motion analysis," *IEEE Transactions on Signal Processing*, vol. 54, no. 3, pp. 809–822, 2006.

[26] ——, "Geometric-polar tracking from bearings-only and Doppler-bearing measurements," *IEEE Transactions on Signal Processing*, vol. 56, no. 11, pp. 5540–5554, 2008.

[27] S. K. Rao, "Pseudo-linear estimator for bearings-only passive target tracking," *IEE Proceedings - Radar, Sonar and Navigation*, vol. 148, no. 1, pp. 16–22, 2001.

[28] N. González-Prelcic, A. Ali, V. Va, and R. W. Heath Jr., "Millimeter-wave communication with out-of-band information," *IEEE Communications Magazine*, vol. 55, no. 12, pp. 140–146, 2017.

[29] R. Alieiev, T. Hehn, A. Kwoczek, and T. Kürner, "Predictive communication and its application to vehicular environments: Doppler-shift compensation," *IEEE Transactions on Vehicular Technology*, 2018, early access.

[30] R. C. Daniels, C. M. Caramanis, and R. W. Heath Jr., "Adaptation in convolutionally coded MIMO-OFDM wireless systems through supervised learning and SNR ordering," *IEEE Transactions on Vehicular Technology*, vol. 59, no. 1, pp. 114–126, 2010.

[31] A. Djouama, E. Zöchmann, S. Pratschner, M. Rupp, and F. Y. Ettoumi, "Predicting CSI for link adaptation employing support vector regression for channel extrapolation," in *Proc. of the 20th International ITG Workshop on Smart Antennas (WSA 2016)*. VDE, 2016, pp. 1–7.

[32] V. Va, J. Choi, T. Shimizu, G. Bansal, and R. W. Heath Jr., "Inverse multipath fingerprinting for millimeter wave V2I beam alignment," *IEEE Transactions on Vehicular Technology*, vol. 67, no. 5, pp. 4042–4058, 2018.

[33] M. Rockl, T. Strang, and M. Kranz, "V2V communications in automotive multi-sensor multi-target tracking," in *Proc. of IEEE 68th Vehicular Technology Conference (VTC-Fall)*, 2008, pp. 1–5.

[34] R. J. Carroll, D. Ruppert, C. M. Crainiceanu, and L. A. Stefanski, *Measurement error in nonlinear models: a modern perspective*. Chapman and Hall/CRC, 2006.

[35] G. Battistelli, L. Chisci, C. Fantacci, A. Farina, and A. Graziano, "Networked target tracking with Doppler sensors," *IEEE Transactions on Aerospace and Electronic Systems*, vol. 51, no. 4, pp. 3294–3306, 2015.

[36] B. Hassibi, A. H. Sayed, and T. Kailath, *Indefinite-Quadratic Estimation and Control: A Unified Approach to H2 and H-infinity Theories*. SIAM, 1999, vol. 16.

[37] T. Kailath, A. H. Sayed, and B. Hassibi, *Linear estimation*. Prentice Hall, 2000.